Eur. Phys. J. B **55**, 337–345 (2007)
DOI: 10.1140/epjb/e2007-00077-7

THE EUROPEAN PHYSICAL JOURNAL B

Effect of the substrate ferroelastic transition on epitaxial $La_{0.7}Sr_{0.3}MnO_3$ films grown on $LaAlO_3$

A. Geddo Lehmann[1], C. Sanna[1], N. Lampis[1], F. Congiu[1], G. Concas[1], L. Maritato[2,a], C. Aruta[3], and A.Yu. Petrov[2]

[1] Dipartimento di Fisica, Università di Cagliari and CNISM, S.P. Monserrato-Sestu km 0.700, 09042 Monserrato (CA), Italy
[2] INFM "Coherentia" and INFM-UdR di Salerno, Dipartimento di Fisica, Università di Salerno, via S. Allende, 84081 Baronissi (SA), Italy
[3] Coherentia CNR-INFM and Dipartimento di Ingegneria Meccanica, Università di Roma "TorVergata", via del Politecnico 1, 00133 Roma, Italy

Received 19 June 2006 / Received in final form 20 November 2006
Published online 22 March 2007 –

Abstract. Thin films of $La_{0.7}Sr_{0.3}MnO_3$ were grown by molecular beam epitaxy on (001)$LaAlO_3$ crystals. High resolution X-ray diffraction analysis proves the presence of twins in the films at room temperature, showing that the twin structure of the substrate which forms at the $Pm\bar{3}m \rightarrow R\bar{3}c$ ferroelastic transition at $T_F = 813$ K served as a template for the film microstructure. Magnetic measurements indicate a thermomagnetic irreversibility which is ascribed to the quenched disorder related to twinning and discussed in terms of coexisting ferromagnetic and spin disordered regions connected with the undeformed domain cores and strained domain walls respectively.

PACS. 75.47.Gk Colossal magnetoresistance – 73.50.-h Electronic transport phenomena in thin films

1 Introduction

There is increasing evidence that the complex behaviour of transition metal oxides (TMO) is triggered by the interplay between electron correlations and structural quenched disorder, namely random or correlated frozen deviations from periodicity [1,2]. The Mn-containing systems $Ln_{1-x}Ak_xMnO_3$ (Ln is a rare earth or lanthanide; Ak is a divalent alkali as Ba, Sr or Ca), which crystallize in variants of the simple perovskites structure ABO_3, are paradigmatic TMO and the study of the effect of disorder on their properties is receiving great attention.

Known mainly for the giant effect which a magnetic field H has on their charge transport, giving rise to the so called colossal magnetoresistance (CMR), which is a gigantic resistance decrease induced by H [3,4], the $Ln_{1-x}Ak_xMnO_3$ phases are derived from the end-member ($x = 0$) compounds $LnMnO_3$, antiferromagnetic Mott-Hubbard or charge transfer insulators, by hole doping via heterovalent chemical substitutions at lanthanide site. The resulting temperature-hole (T, h) phase diagram contains competing electronic, magnetic and structural phases. The two main competing phases are a charge ordered (CO)/orbital ordered (OO) antiferromagnetic insulator (AFI) and a ferromagnetic metal (FM) [5,6], the latter described within the Zener model for charge delocalization via parallel spin alignment [7–9]. What phase is realized on hole doping can be controlled via two key parameters, the effective one electron e_g bandwidth W related to the transfer integral of the conducting e_g electrons between neighbouring Mn sites [7–9], and the variance σ_A^2 of the A-cations radius distribution defined as $\sum y_i r_i^2 - \langle r_A \rangle^2$ [10], where y_i and r_i are the fractional occupancies and ionic radii of the i cations and $\langle r_A \rangle$ is the mean A-site cation size. The bandwidth W depends only on $\langle r_A \rangle$, which modifies the tendency towards long range lattice distortions of the cubic perovskite, quantified by the tolerance factor of Goldschmidt $t = (\text{A-O})/\sqrt{2}(\text{B-O})$ (A, B, and O are the ionic radii within the ABO_3 perovskite) and the related Mn-O-Mn bond bending. For smallest bending and large W (i.e. $La_{1-x}Sr_xMnO_3$) there are the ferromagnetic metals with the highest Curie points T_C, for intermediate W ($Nd_{1-x}Sr_xMnO_3$and $La_{1-x}Ca_xMnO_3$) one finds reduced values of T_C with thermally driven metal to insulator transitions and high values of CMR, while for small bandwidth ($Pr_{1-x}Ca_xMnO_3$) there are only insulating phases [6]. The variance σ_A^2, on the contrary, describes the local deviations from the average A-site translational periodicity and measures the degree of quenched point-like disorder. It has been pointed out that strong local deviations from the average structure may drastically alter the balance between the CO/OO AFI and FM phases with respect to the "clean limit" [5]. With an increasing amount

[a] e-mail: maritato@sa.infn.it

of disorder, the long range order of both the two competing CO/OO AFI and FM phases is suppressed and a intervened spin-glass-like insulator appears instead [11,12], while the tendency towards inhomogeneous (phase separated PS) states is enhanced. Notably, near the ferromagnetic/spin glass boundary, where the two phases might coexist, also the CMR is most enhanced [12,13]. The similarity with other TMO is often remarked and, in particular, it has been argued that, under suitable conditions, the glassy state in the underdoped regime of cuprates, with nanoscale superconducting puddles, might lead to "colossal" effects, analog of CMR in manganites [14].

In many real samples, wether ceramics, single crystals, thin films, the disorder is generated not only by point-like defects introduced by chemical substitutions, but also by extended defects, as dislocations or grain boundaries or twin boundaries. In particular, twinning is widespread in single crystals of perovskite-type oxides, owing to the usual presence of ferroelastic transitions. The spontaneous formation of domain structure in bulk ferroelastic materials under cooling below the transition temperature is well understood from a thermodynamic point of view [15]. Ferroelastic crystals display characteristic domain patterns on a mesoscopic length scale. Twin states (precisely transformation twins or ferroelastic domains) are separated by twin boundaries, which can host severe structural distortion. The crystallographic orientation of such boundaries is fixed by twin laws, so that the positions of the distorted regions are correlated. The role of structural distortion in promoting inhomogeneities in manganites has been studied [16], supporting the idea of a possible crystallographic-texture-driven enhanced metal-insulator PS.

Twinning can arise also in epitaxial films, either from strain relaxation mechanisms [17,18] or as a consequence of the use of a suitable substrate, like the perovskite $LaAlO_3$. At room temperature $LaAlO_3$ is rhombohedral (space group$R\bar{3}c$), because of a cooperative antiferrodistortive rotation of AlO_3 octahedra about one of the three-fold symmetry axes of the undistorted cubic cell. This $R\bar{3}c$ phase is ferroelastic [19–22], because it results from a structural transition of a parent phase $Pm\bar{3}m$ at the critical temperature recently redetermined as $T_F = 813$ K [23]. Therefore multiple orientation states exist below T_F in $LaAlO_3$ crystals in the absence of mechanical stress. A crystal with twinning has structured crystallographic morphology, like roof-like facets, and crystals of $LaAlO_3$ used as substrates commonly twin [24,25]. The twin structure of the substrate is expected to influence the epitaxial growth or even to act as template for producing a microstructured film. For instance, twins have been directly observed, by transmission electron microscopy, in $La_{0.7}Ca_{0.3}MnO_3$ films obtained by metal-organic deposition process and considered to be the "prolongation" of those formed at T_F in the substrate [26]. Twin boundaries in the $LaAlO_3$ substrate have been demonstrated to cause a clear splitting of the manganite magnetic domains in $YBa_2Cu_3O_{7-x}/La_{0.67}Sr_{0.33}MnO_3$ bilayers grown by high pressure sputtering, leading to twinned films with in-plane magnetization domains separated by out-of-plane magnetic structures pinned at twin boundaries [27]. The role of the twinned substrate has been discussed also in the case of $La_{0.7}Sr_{0.3}MnO_3$ films grown by pulsed laser deposition, the magnetic pattern of which observed by magnetic force microscopy, either "maze-like" or bubble (both characteristic of out-of-plane magnetization systems), has been ascribed to a sample-dependent substrate domains structure which is realized under different growth conditions [28].

In this work we shall present experiments performed on of thin epitaxial films of $La_{1-x}Sr_xMnO_3$ with $x = 0.3$ deposited on ferroelastic $LaAlO_3$ by Molecular Beam Epitaxy (MBE) at 973 K, i.e. above T_F of $LaAlO_3$. In the bulk, the manganite $La_{0.7}Sr_{0.3}MnO_3$ is isostructural with $LaAlO_3$ at room temperature, with rhombohedral $R\bar{3}c$ cell corresponding to pseudocubic axes $a_{\rm pc} = 0.3873$ nm and $\alpha = 90.26°$ [29]. A rhombohedral distortion is retained at least up to 1173 K [30]. At the deposition temperature, therefore, it is the rhombohedral phase of $La_{0.7}Sr_{0.3}MnO_3$ that growths epitaxially on the untwinned paraelastic structure of $LaAlO_3$, i.e. on (100) cubic crystallographic facets. Strained growth of rhombohedral $La_{0.7}Sr_{0.3}MnO_3$ on a cubic substrate is known to be tetragonal [17]. The room temperature lattice mismatch with $LaAlO_3$, evaluated from the pseudocubic edges $a^s_{\rm pc}$ and $a^f_{\rm pc}$ of the substrate and the film, is $m = -2.2\%$ leading to a strained cell with $c/a > 1$. In the absence of structural change of the substrate on lowering temperature in the MBE deposition chamber, the tetragonal symmetry of the $La_{0.7}Sr_{0.3}MnO_3$ film can be retained down to room temperature for film thickness below the critical value t_c, which for $La_{0.7}Sr_{0.3}MnO_3$ on $LaAlO_3$ has been estimated in 15–20 nm [31,32]. The structural features of $La_{0.7}Sr_{0.3}MnO_3$ on $LaAlO_3$, however, will be complicated by the formation of the rhombohedral twinning in the substrates during cooling down to room temperature. It is the aim of this paper to discuss the relationships between the crystallographic features and the magnetic properties of the manganite layers, with reference to a possible microstructure induced by the ferroelastic transition of the substrate. To this purpose, we shall present high-resolution X-ray diffraction analyses of the epitaxial films, discuss crystallo-optics images of the substrates twin structure, and analyse magnetization measurements performed with a SQUID magnetometer.

2 Samples and experimental procedure

The thin $La_{0.7}Sr_{0.3}MnO_3$ films LSMO9 and LSMO20 (in which the numbers refer to the thickness in nanometers) have been deposited by MBE, using a codeposition procedure in which the elemental rates of La e-beam sourced, Sr and Mn effusive cells have been carefully controlled to obtain the desired sample composition. The peculiarity of the MBE is the possibility to achieve the in-situ formation of the perovskites at very low oxygen pressure without post annealing treatment. In our case, a mixture of O_2 +5% ozone at a total pressure $P = 2.63 \times 10^{-2}$ Pa was

employed. The atmosphere composition inside the deposition chamber has been controlled by mass spectroscopy. The reflected high energy electron diffraction (RHEED) analysis has been performed during the growth process to check the structural properties of the films. Details of this surface analysis and on composition check by energy dispersive X-ray spectroscopy (EDS) have been already reported [32]. The $LaAlO_3$ (100) substrates have been held at 973 K during growth, i.e. above their ferroelastic transition temperature T_F. After deposition, samples were cooled to room temperature passing through T_F. The onset of macroscopic twinning in $LaAlO_3$, as evidenced by birefringence imaging and measurement [23], occurs approximately at 803 K, i.e. 10 K below the $Pm\bar{3}m \rightarrow R\bar{3}c$ transition temperature, with a domain structure rather mobile above 750 K while quite stable below 750 K.

High resolution X-ray diffraction and magnetization measurements were carried out before samples manipulation for optical observations of the substrate ferroelastic domain structure. For optical observation of the domain structure at room temperature, $LaAlO_3$ crystals were freely mounted, before and after the film deposition, on the rotary stage of a Leitz Orthoplan Pol microscope with crossed polars. Samples were mechanically polished on the backside with respect to the face on which the films were deposited and cleaned by suitable solvents. To the aim of releasing possible strain induced by mechanical polishing, while preventing domains motion, samples were annealed for several hours at the quite low temperature of 623 K. The crystallographic characterization of LSMO20 and LSMO9 was performed by high resolution X-ray diffraction, through the analysis of ω-scans and reciprocal space maps, using a four circles diffractometer (Bruker D8 Discover) with Cu anode. The magnetization measurements were performed using a Quantum Design MPMS5 XL5 SQUID magnetometer, equipped with a superconducting magnet producing fields up to 50 kOe and calibrated using a Pd standard; the sensitivity for the magnetic moment is 10^{-8} emu.

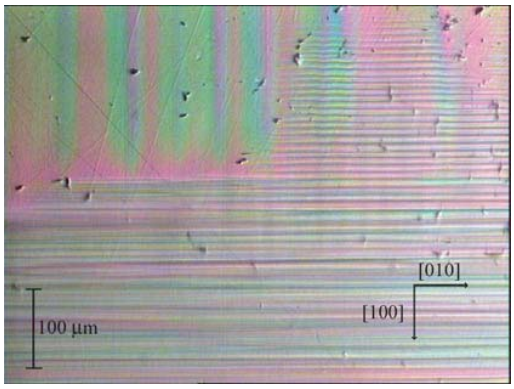

Fig. 1. As received $LaAlO_3$ substrate under crossed polars (magnification $10x$). Domains are visible as coloured stripes running along the [100] (up left) and [010] directions.

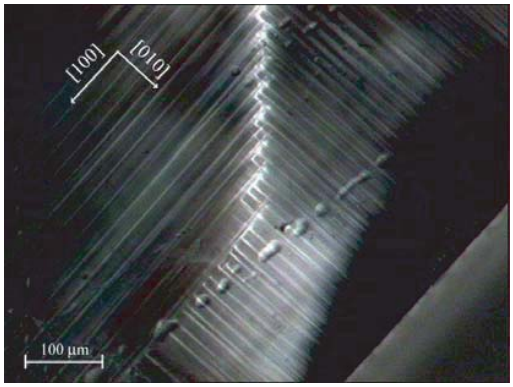

Fig. 2. A region of the substrate at extinction position ($10x$). The observed domain pattern is likely to be due to the presence of two incompatible chevron orientations, which can be distinguished by their {100} domain walls, namely (100) and (010) pseudocubic planes respectively. The high lattice strain associated with the boundary between the two chevron orientations causes the residual birefringence contrast in the central part of the micrograph.

3 Results and discussion

3.1 Optical characterization of the ferroelastic domain structure of the $LaAlO_3$ substrates

When $LaAlO_3$ crystals are observed in transmission under crossed polarizer and analyzer, differently oriented rhombohedral domains give rise to a birefringence contrast. From symmetry arguments it can be shown that for $(001)_{pc}$ $LaAlO_3$ platelets, such domains are at position of extinctions at 45° (i.e. when the $[110]_{pc}$ direction is rotated of 45° with respect to analyzer and polarizer). The observed birefringence patterns can be rationalized with reference to the crystallography of the $LaAlO_3$ twin structure [21,22,25]. In the $Pm\bar{3}m \rightarrow R\bar{3}c$ symmetry change occurring in $LaAlO_3$, which corresponds to the ferroic species $m3mF3m$, in the Aizu notation [33], transformation twins form on cooling below T_F due to the choice of four equivalent triad axes of the $m3m$ class about which AlO_3 octahedra rotation can occur. Given the four pure twin domain states, with ternary axis along [111], [1-11], [–111], [11-1], there are six possible pairs of domain states that can meet to form a domain wall. For each of the six pairs there are two possible orientations of domain walls, one of the form $\{100\}_{pc}$ and one of the form $\{110\}_{pc}$. This produces a total of twelve physically distinguishable couples of twin domain orientations. In the case of a $(001)_{pc}$ oriented platelet, like our $LaAlO_3$ substrates, walls belonging to the form $\{100\}_{pc}$ are normal to the deposition surface or parallel to it, while walls of the form $\{110\}_{pc}$ are either normal or inclined at 45° with respect to the deposition face.

Figure 1 shows the typical domain pattern of an as-received substrate before deposition. The coloured stripes parallel to $[100]_{pc}$ and $[010]_{pc}$ are identified with domains with walls of the form $\{110\}_{pc}$, inclined at 45° to the $(001)_{pc}$ surface. The width of these domains varies from about 5 μm to 50 μm. Needles are present at intersection of stripes along the $[100]_{pc}$ and $[010]_{pc}$. A region of the substrate at extinction is shown in Figure 2. The observed

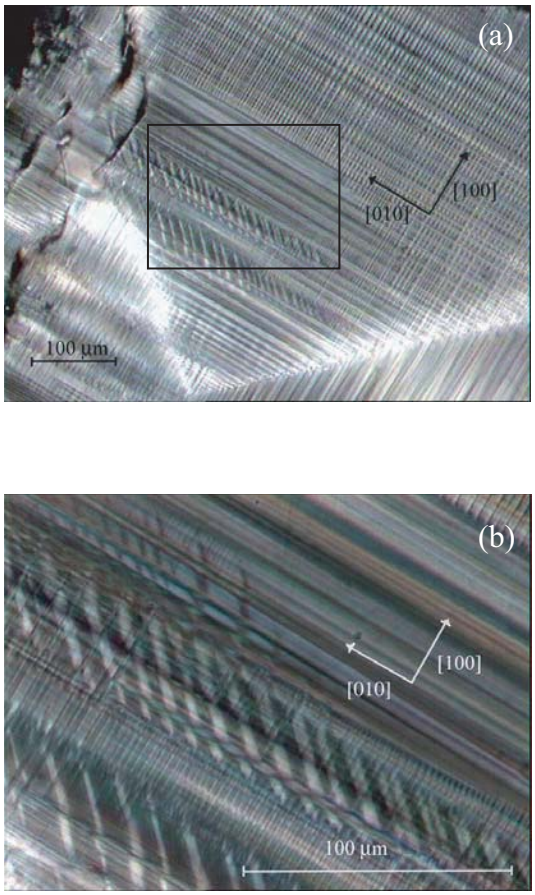

Fig. 3. Substrate with LSMO20 film under crossed polars. (a, $10x$) Striped domains along [100] and [010], with widths as small as 5 μm. The marked region in (a) is shown in (b) at higher magnification ($32x$), to evidence the presence of stripes both along [100] , [010] and along [110], these latter with domain walls of the form {110} perpendicular to the film surface, i.e. (110) planes. Also the interception of incompatible chevron is present.

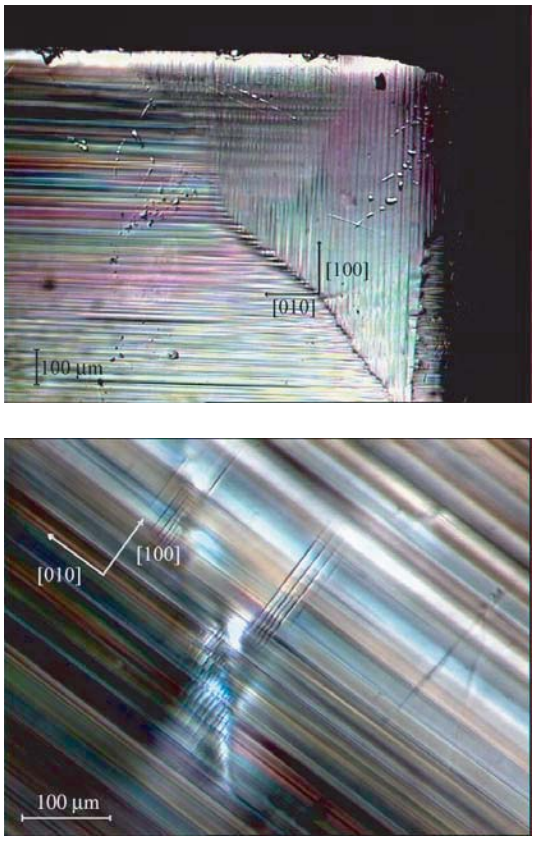

Fig. 4. Substrate with LSMO9 film under crossed polars. (a, $4x$) Domains running parallel to [100] and [010] direction are visible. (b, $10x$) LSMO9 near extinction revealing highly strained regions at 90° walls interception.

domain pattern is likely to be due to the presence of two incompatible "chevron" orientations [21], which can be distinguished by their $\{100\}_{\rm pc}$ domain walls, namely (100) and (010) pseudocubic planes respectively. The high strain associated with the boundary between the two chevron orientations causes the residual birefringence contrast in the central part of the micrograph. Substrates received twin-free were found to display the same kind of domain structure if cycled in temperature in the MBE chamber.

The two substrates with the deposited LSMO epilayers were observed with the latter upside. This information is given for the sake of completeness. Figure 3 shows the substrate with deposited LSMO20. As can be seen, after the deposition cycle the ferroelastic domains in $LaAlO_3$ are still present, and stripes are visible along $[100]_{\rm pc}$ and $[010]_{\rm pc}$, with widths of about 5 μm (Fig. 3a). The interception of incompatible chevrons is also present. At higher magnification (Fig. 3b) stripes both along $[100]_{\rm pc}$, $[010]_{\rm pc}$ and along $[110]_{\rm pc}$ are revealed, these latter with domain walls of the form $\{110\}_{\rm pc}$ perpendicular to the film surface, i.e. $(110)_{\rm pc}$ planes. Figure 4 shows two details of the substrate with LSMO9. Domains running parallel to $[100]_{\rm pc}$ and $[010]_{\rm pc}$ direction are visible (Fig. 4a) and, near extinction position (Fig. 4b), highly strained regions at interception of 90° walls are revealed.

3.2 High resolution X-ray diffraction analysis

To investigate the effect of the substrate ferroelastic transition on the deposited LSMO20 and LSMO9 films, room temperature high resolution X-ray analyses were performed. Rocking curves (or ω-scans) and reciprocal space maps (RSM), two of the typical reciprocal space scans in thin films characterization by X-ray diffraction, are powerful tools for the study of twinned crystals in which the reciprocal lattice vectors representing a set of equivalent lattice planes in different twins are not parallel. To perform a rocking curve, as clearly explained by Harrison et al. [21], a suitably oriented crystal of $LaAlO_3$ is placed close to the diffraction condition, with the reciprocal lattice vectors of different twins lying within the scattering plane. The crystal is then rotated by an angle ω about an axis perpendicular to the scattering plane, to bring into the diffracting condition one twin at a time. A rocking curve, which is a plot of integrated intensity as a function

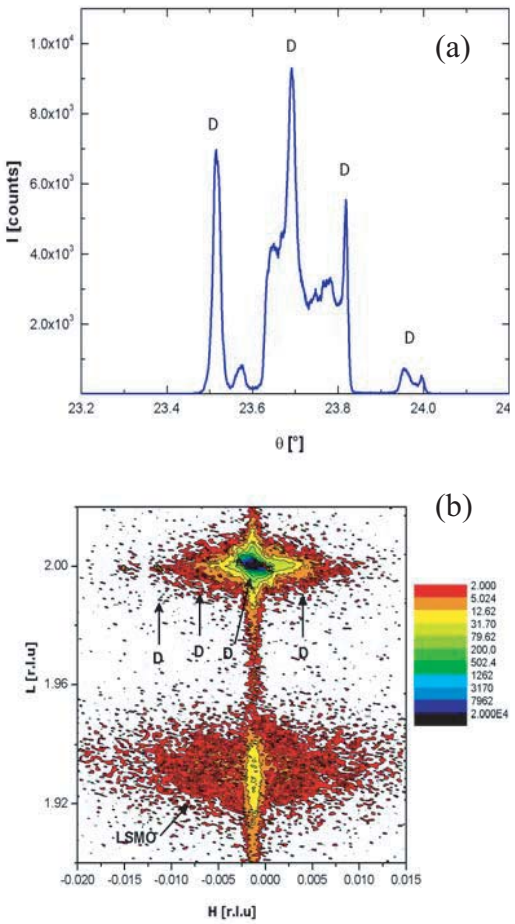

Fig. 5. (a) Rocking curve of $LaAlO_3$ substrate of LSMO20 around the $(002)_{pc}$ reflection. Four domains marked as D are visible. (b) Reciprocal space map around the $(002)_{pc}$reflection of the substrate for LSMO20. Domains in the substrate visible along q_z = cost =2 are indicated with D.

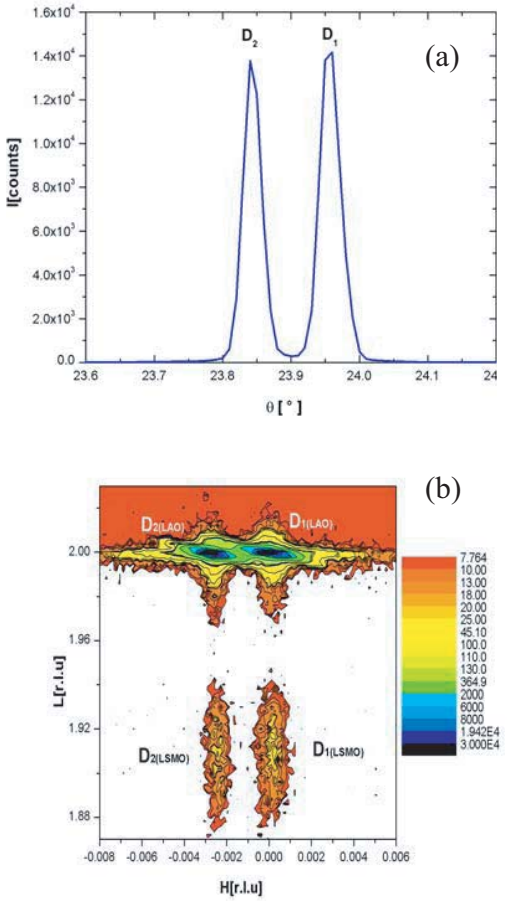

Fig. 6. (a) Rocking curve of $LaAlO_3$ substrate of LSMO9 around the $(002)_{pc}$ reflection; (b) Reciprocal space map around the $(002)_{pc}$ reflection of the substrate for LMSO9. The two domains in the substrate visible along $q_z = 2$ are clearly duplicated in the film at lower q_z.

of ω, will show individual peaks corresponding to each of the twin domains. The angular difference between the peak positions in the rocking curves is related to the angular difference between the reciprocal lattice vectors in different domains. Simulated rocking curves of rhombohedral $LaAlO_3$ crystals in $(001)_{pc}$ orientation have been reported for different twin structures [21], i.e. for crystals containing different aggregates of ferroelastic domains, and can be compared with our X-ray experiments. A reciprocal space map consists of iterated ω scans at fixed 2ϑ values, for a certain range of $\omega/2\vartheta$, around a given reciprocal node of the paraelastic cubic phase of $LaAlO_3$, or, alternatively, of iterated q_x scans (transverse scan) for a certain range of the q_z coordinate (longitudinal scan) around the corresponding point (q_x, q_z). The resulting two-dimensional map will contain the scattered intensity associated with the Bragg nodes of the rhombohedral twins.

Figure 5a shows the rocking curve of the $(002)_{pc}$ reflection of he $LaAlO_3$ (001) substrate after deposition of the LSMO20 film. Besides the peak doubling for the presence of both $k\alpha_1$ and $k\alpha_2$ wavelengths, the scan profile indicates that four different orientational variants D enter in Bragg conditions during the ω scan and contribute to the recorded intensity [21]. Figure 5b displays the corresponding RSM. Four domains D of the substrate can be appreciated along a one-dimensional section at q_z = cost ≈ 2. The LSMO20 diffusion around the $(002)_{pc}$ film node is recognized at a lower q_z value. We see that the LSMO20 diffuse scattering is anomalously wide along q_x, with a full width at half maximum *FWHM* value mainly influenced by the twin structure of $LaAlO_3$ substrate. This result is analogous to what found in case of Ca-doped $La_{0.7}Ca_{0.3}MnO_3$ film deposited on $LaAlO_3$ by RF magnetron sputtering, also twinned [34]. This indicates the presence of different crystallographic orientations in LSMO20, as in the substrate, not well resolved due to the complex structure of the substrate rocking curve.

For LSMO9, the rocking curve of the $(002)_{pc}$ reflection of the substrate, collected with the use of a 2-bounces V-groove monochromator, is shown in Figure 6a. Its simpler profile means that the same Bragg condition is valid for two domain states at a time, giving rise to only two

peaks [21]. The corresponding RSM around the $(002)_{pc}$ reflection is reported in Figure 6b. The domains are clearly visible and well resolved both for the substrate and for the film. We remark that the domain separation along the reciprocal coordinate q_x in LSMO9 is the same as in the $LaAlO_3$ substrate, which indicates that twins in the epilayer are in strict connection with those in $LaAlO_3$. Actually, the observed twins must have formed in LSMO films when domains raised in $LaAlO_3$ substrate just below the cubic to rhombohedral transition temperature T_F, with the domain structure of the substrate acting as template for the manganite film, a result which is in line with recent findings concerning the role of the substrate ferroelastic transition on the presence of twinning in LSMO films [27,35]. It is possible that the substrate transformation acts as a driving force for the transformation of the $La_{0.7}Sr_{0.3}MnO_3$ film towards its bulk rhombohedral symmetry and that the twin law for the $Pm\bar{3}m \rightarrow R\bar{3}c$ symmetry change is respected in the film, as it would have been in the bulk. If this would be the case, the observed domains in the manganite films would be correctly called transformation twins. This is different to what happen $La_{0.7}Ca_{0.3}MnO_3$ on $SrTiO_3$ when this latter undergoes the cubic-tetragonal ferroelastic transition at 105 K [36]. Also in this case domains are formed in the manganites film, however without crystallographic correlation with those of the substrate. The origin of the herewith discussed twinning differs also from that of the domains found in $La_{1-x}Sr_xMnO_3$ coherently grown on untwinned substrates, like (001)-oriented $SrTiO_3$ [17,18], which are explained in terms of strain relaxation mechanisms. According to this explication, the part of the elastic energy due to the lattice mismatch is diminished by the formation of misfit dislocations at the film/substrate interface, while the part which is related to the shear strain, and which results from the rhombohedral symmetry of $La_{0.7}Sr_{0.3}MnO_3$ at room temperature, when it is matched onto a cubic substrate, is reduced by the formation of structural domains with an alternating sign of shear. Such a structural domain pattern can be also called a "twin pattern", since the crystallographic orientation of neighboring domains is similar to common twins. However, these domains are more similar to mechanical twins than to transformation twins.

3.3 Magnetic properties

Different spin disordered systems, as spin glasses (SG) and cluster spin glasses (CSG), are characterized by a cusp in the zero field cooling (ZFC) magnetization (M_{ZFC}), indicating the freezing of the spins at the freezing temperature T_f (determined as the temperature of the maximum of M_{ZFC}), and by a separation between ZFC and field cooling (FC) magnetization (M_{FC}) at the irreversibility temperature T_{irr}, which indicates the onset of irreversibility [37]. Therefore, to probe the presence of irreversible thermomagnetic features induced by the correlated disorder associated to twinning, the two LSMO films were studied by ZFC and FC magnetization versus temperature measurements for 4 K $< T <$ 400 K [38].

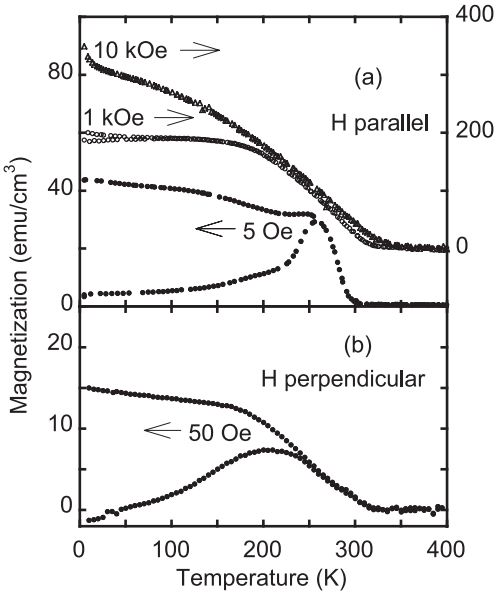

Fig. 7. Magnetization vs. temperature of the LSMO20 film. (a) With applied field parallel to the film plane, $H = 5$ Oe (dots, left axis), 1 kOe (open circles, right axis), 10 kOe (open triangles, right axis); (b) with applied field perpendicular to the film plane, $H = 50$ Oe (dots). For each value of H, the lower and upper curves show the ZFC and FC magnetization, respectively.

The ZFC-FC curves of the LSMO20 film are plotted in Figure 7a for applied field parallel to the film plane (H||). The M_{ZFC} at low field (5 Oe) shows a peak at $T_f = 260 \pm 5$ K; the corresponding FC curve separates at a slightly higher temperature, which is therefore designed as the irreversibility temperature. After an initial slight decrease, with a broad minimum in coincidence with the inflection point of the ZFC curve, M_{FC} increases at low temperature. The ZFC peak disappears in the magnetization at 1 kOe, while a separation is still present at temperature lower than $T_{irr} = 70$ K. The ZFC-FC separation vanishes at 10 kOe. For applied field perpendicular to the film plane (H$\perp$), the ZFC-FC irreversibility is qualitatively similar, as it can be argued from Figure 7b, which shows the case of $H = 50$ Oe, with the maximum of M_{ZFC} giving $T_f = 205 \pm 5$ K.

The ZFC and FC magnetization of the LSMO9 film for H|| and H$\perp$ are shown in Figures 8a and 8b respectively. A first peculiar feature can be noticed for this sample: with applied field up to 1 kOe, the ZFC-FC irreversibility is observed almost in the whole measured temperature range. The more evident splitting between M_{ZFC} and M_{FC} takes place in the low temperature range, i.e. below the major rising of the magnetization (see for instance Fig. 8b, $H = 500$ Oe). Nevertheless, the two curves remain separated up to about 350 K. This feature is more evident for the case with H$\perp$ (see Fig. 8b), but is also present for H|| (Fig. 8a). The high temperature irreversibility is not more detectable for $H = 10$ kOe. The second salient feature of

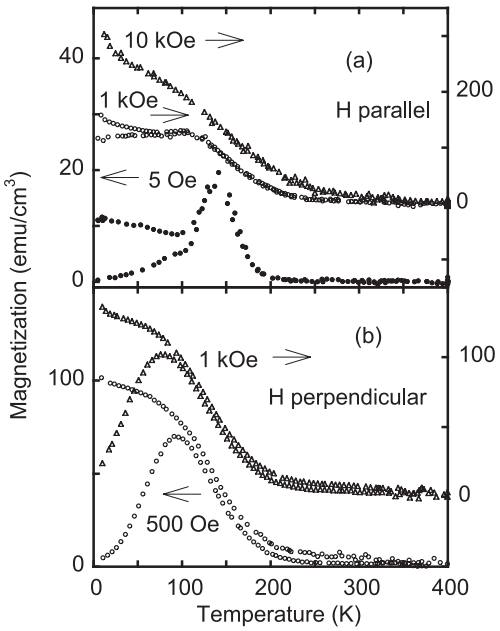

Fig. 8. Magnetization vs. temperature of the LSMO9 film. (a) With applied field parallel to the film plane, $H = 5$ Oe (dots, left axis); 1 kOe (open circles, right axis), 10 kOe (open triangles, right axis); (b) with applied field perpendicular to the film plane, $H = 500$ Oe (open circles, left axis), 1 kOe (open triangles, right axis). For each value of H, the lower and upper curves show the ZFC and FC magnetization, respectively.

this thinner film is that, for H|| with $H = 5$ Oe, the peak at 140 K of M_{ZFC} is associated with a coincident peak of M_{FC}; this behaviour is still observable at 1 kOe, with the peak temperature shifted to about 100 K. The peaks disappear with an applied field of 10 kOe. For H$\perp$, the ZFC curves show the peak with fields up to 1 kOe, but there is no observable concomitant anomaly in the FC curves.

The Curie temperature (T_C) for LSMO20 is 289 ± 1 K, as evaluated from the low field magnetization (with $H = 5$ Oe) fitted by the mean field theory expression $M(T) = A(T_C - T)^{1/2}$ in the vicinity of the transition [39]. The Curie temperature is notably lower than the bulk value of 378 K. Its reduction can be related to the disorder due to twin boundaries and to other extended defects (dislocations) which may be present, because the LSMO20 thickness is above the critical value for pseudomorphic growth. In addition, the effect of epitaxial strain on T_C should be considered. Strain effect in manganites has been modeled [40,41], by properly taking into account the modification it induces in the Mn-O-Mn bond angle ϑ and in the Mn-O bond lenght d, which both appear in the empirical formula for the hopping of electrons between two neighbour Mn sites, which controls $T_C, t \propto d^{-3.5} \sin \vartheta/2$ [42]. It was found that also for compressive strain (as it is for $La_{0.7}Sr_{0.3}MnO_3$ on $LaAlO_3$) a reduction of the transition temperature T_C can occur, in contrast to the simpler interpretation in terms of contraction of the in-plane Mn-O bond length d alone, which should lead to an increase of the electron in-plane hopping t and thus T_C. Actually, however, since our samples have been proved to be structurally partially relaxed, we expect that strain plays a minor role on T_C. Last, an important factor to be considered for the decrease of the Curie temperature T_C in thin films is the finite size effect [43,44]. The finite film thickness d limits the divergence ξ of the spin-spin correlation lenght at T_C, which results in a decrease of T_C with respect to the bulk value for $d < \xi$. For instance, the finite size scaling of T_C has been reported for the lanthanum cobaltite $La_{0.7}Sr_{0.3}CoO_3$ thin films [45] for thickness between 2.6 nm and 42 nm.

For the LSMO9 film, the data analysis described for LSMO20 would lead to $T_C = 186 \pm 1$ K. Since this sample presents irreversibility, for fields as high as 1 kOe, up to 350 K, we prefer to indicate this temperature as T_C^*, in order to emphasize that it represents the temperature that marks the passage between two magnetic ordering regimes. This point will be discussed in more detail in the following.

A separation between M_{ZFC} and M_{FC} has been already reported for $La_{0.7}Sr_{0.3}MnO_3$ film grown on $LaAlO_3$ by sputtering [46] with thickness of 600 nm and ascribed to a spin-glass like behaviour caused by the competition between ferromagnetism and antiferromagnetism, as a direct consequence of the random distribution of Mn^{3+} and Mn^{4+} ions, without mention to the possible role of the substrate-induced twinning on the observed lacking of true magnetic long range order. To the best of our knowledge, the magnetism of thinner films has not yet been discussed in this contest. A cusp in the M_{ZFC} at T_f, and a separation between M_{ZFC} and M_{FC} at T_{irr} are both present in the magnetization curves of LSMO20 (see Fig. 7). Even though not conclusive, these features make a strong case in favour of spin-glass-like properties of LSMO20. Moreover, because it is also possible to identify a Curie temperature T_C above both T_f and T_{irr}, we suggest that the irreversible magnetic behaviour of LSMO20 can be ascribed to a reentrant spin glass (RSG). As described by Ito [47], a RSG has to be considered a mixed phase of the long range ferromagnetic phase and the SG phase. The mechanism of the RSG transition is that, when the long range order is established at T_C, some amount of disordered (not aligned) spins exists in the long range ferromagnetic network. With decreasing temperature, even some of the spins participating to the long range order escape from the ordered network, resulting in an increasing amount of the frustrated spins. On further lowering temperature, the frustrated spins freeze at T_f.

We would attempt to relate the observed magnetic behaviour to the microstructure of LSMO20. We may suppose that double-exchange couplings are dominant inside each structural domain and that frustration appears in a "transition region" between them, which we identify with the twin walls. In other words, a coreshell-type structure is proposed, in which the core is ferromagnetic and metallic while the shell is spin disordered and insulating. This picture has already been used for $La_{0.7}Sr_{0.3}MnO_3$ nanoparticles with surface spin-glass layers formation [48] and for polycrystalline films of $La_{0.7}Ca_{0.3}MnO_3$ which, beside the ferromagnetic core, display spin glass phases related to

grain boundaries and grain surfaces [49]. The depicted microstructural description of the twinned LSMO film is reminiscent of the *two-phase scenario*, according to which FM regions (in our case inside the twins) and AFI regions (induced in our case by locally enhanced strain at twin boundaries) coexist in manganites with CMR [50]. In particular, this description refers to the model of Ahn et al. [16], in which the insulating phase has a short- or long-wavelengths lattice distortion, and the metallic phase is undistorted, with emphasis put on the primary importance of structural aspects in causing the multiphase coexistence.

The same coreshell model is also useful to explain the irreversibility observed in the thinner LSMO 9 film well above T_C^*. The observed high temperature thermomagnetic irreversibility in LSMO9 is consistent with the formation of frozen FM clusters within the undistorted metallic core of the structural domains at $T_{irr} = 350$ K. This temperature is not far from the bulk Curie point, a result that seems to indicate that the inner part of the twins is almost free from defects due to relaxation, as it should be, given the small film thickness. The relevant presence of the distorted paramagnetic shells in LSMO9 prevents the occurrence of a long range ferromagnetic ordering between the clusters for $T_C^* < T < T_{irr}$. A global ferromagnetic state develops in the film only at T_C^*, as evidenced by the strong increase of the FC magnetization. The presence of ferromagnetic clusters in manganites for temperatures above T_C has been recently predicted [13], thus introducing different temperature regimes: a high-T regime where the system is magnetically disordered, an intermediate-T range with preformed ferromagnetic clusters with uncorrelated order, and a low-T regime where the clusters grow in size giving a globally ferromagnetic behaviour. The observation of the intermediate-T regime in $La_{1-x}Sr_xMnO_3$ phases has been reported in the case of single crystal with Sr doping up to $x = 0.16$ and discussed in terms of a Griffiths phenomenon [51], suggested to represent a generic feature of manganite systems, not restricted to the weakly doped regime, when the structural distortions are sufficiently strong to allow for the bond disorder to be completely quenched. Actually, previous observations on optimally doped ($x = 0.3$, 0.4) single crystals have been claimed to be consistent either with a *two phase scenario* [50] or with the existence of the intermediate-T regime [52].

As it concerns the anomalous behaviour of the M_{FC} at low field H||, we note that the same feature has been already reported for $La_{0.7}Sr_{0.3}MnO_3$ films on $LaAlO_3$ [53] and ascribed to a spin reorientation transition, an interpretation which stands on the assumption of a substrate induced compressive in-plane strain. This assumption is correct for defect free heteroepitaxial system, but questionable for heavily twinned substrate and microstructured epilayer, which can not be treated as single crystals. Moreover, at a closer look, also LSMO20 exhibits this kind of anomaly, even though much less evident (Fig. 7), with the shallow minimum of M_{FC} at 225 K. This result contrasts with the predicted thickness dependence of the spin reorientation transition temperature, which has been shown to decrease for increasing film thickness [54]. Since the anomaly in the M_{FC} curve is only observed for $LaAlO_3$ substrate [53], while it is absent for untwinned $SrTiO_3$, we wonder if this feature could be instead related to the substrate induced microstructure of the manganite film and in particular to a crystallographic-texture-driven phase separation, an hypothesis that, we remark, that for Ca-doped films has already received some consideration [55–57]. Further investigations are needed to clarify this point.

4 Concluding remarks

Thin epitaxial films of $La_{0.7}Sr_{0.3}MnO_3$ grown by MBE on $LaAlO_3$ have been studied to evidence the connections between structure, microstructure and physical behaviour. High-resolution X-ray diffraction has shown that twins are present in the $La_{0.7}Sr_{0.3}MnO_3$ epitaxial films at room temperature, clearly resolved in reciprocal space maps and in strict crystallographic connection with those of the substrate. Both the analyzed films are therefore characterized by extended planar defects, whose orientation is fixed by the same twin laws valid for the substrate. The correlated quenched disorder due to twinning has been shown to reflect itself in the magnetic behaviour, leading to a thermomagnetic irreversibility which has been discussed in terms of coexisting ferromagnetic and spin disordered regions within domain cores and domain walls, respectively.

The previous results on twinned epitaxial films stress out the connection between quenched structural disorder and phase inhomogeneity in $La_{0.7}Sr_{0.3}MnO_3$ which, for the large width W of the e_g band, is often described as a canonical double exchange system. Our results can be compared with the already mentioned observations concerning single crystals of the same composition [51], also claimed to be consistent either with the *phase separation scenario*, in contrast to the canonical description, or with the presence of an intermediate-T regime with the formation of a Griffiths phase: since the rhombohedral phase of $La_{0.7}Sr_{0.3}MnO_3$ derives from a paraelastic prototype, single crystals should also be twinned, which invites to a reflection upon the origin of the observed electronic and magnetic inhomogeneity.

References

1. E. Dagotto, Science **309**, 258 (2005)
2. E. Miranda, V. Dobrosavljevic, Rep. Prog. Phys. **68**, 2337 (2005)
3. *Colossal magnetoresistive Oxides* edited by Y. Tokura (Gordon & Breach Science Publishers, 1999)
4. E. Dagotto, *Nanoscale phase separaration and colossal magneto-resistance. The physics of manganites and related compounds* (Springer-Verlag, Berlin, 2003)
5. E. Dagotto, New Journal of Physics **7**, 67 (2005)
6. Y. Tokura, Rep. Prog. Phys. **69**, 797 (2006)
7. C. Zener, Phys. Rev. **82,** 403 (1951)

8. P.W. Anderson, H. Hasegawa, Phys. Rev. **100**, 675 (1955)
9. P.G. de Gennes, Phys. Rev. **118**, 141 (1960)
10. L.M. Rodriguez-Martinez, J.P. Attfield, Phys. Rev. B **54**, 15622 (1996)
11. A. Maignan, C. Martin, G. Van Tandeloo, M. Hervieu, B. Raveau, Phys. Rev. B **60**, 15214 (1999)
12. D. Akahoshi, M. Uchida, Y. Tomioka, T. Arima, Y. Matsui, Y. Tokura, Phys. Rev. Lett. **90**, 177203 (2003)
13. J. Burgy, M. Mayr, V. Martin-Mayor, A. Moreo, E. Dagotto, Phys. Rev. Lett. **87**, 277202 (2001)
14. G. Alvarez, M. Mayr, A. Moreo, E. Dagotto, Phys. Rev. B **71**, 014514 (2005)
15. E.K.H. Salje, *Phase Transitions in Ferroelastic and Co-Elastic Crystals* (Cambridge University Press, Cambridge, 1990)
16. K.H. Ahn, T. Lookman, A.R. Bishop, Nature **428**, 401 (2004)
17. J.L. Maurice, F. Pailloux, A. Barthelemy, O. Durand, D. Imhoff, R. Lyonnet, A. Rocher, J.P. Contour, Philosophical Magazine **83**, 3201 (2003)
18. N. Farag, M. Bobeth, W. Pompe, J.S. Speck, J. Appl. Phys. **97**, 113516 (2005)
19. E.A. Wood, Americ. Mineralog. **36**, 768 (1951)
20. S. Geller, V.B. Bala, Acta Cryst. **9** 1019 (1956)
21. R.J Harrison, S.A.T. Redfern, A. Buckly, E.K.H. Salje, J. Appl. Phys. **95**, 1706 (2004)
22. S. Bueble, W.W. Schmahl, Materials Structures **6**, 140 (1999)
23. S.A. Hayward, F.D. Morrison, S.A.T. Redfern, E.K.H. Salje, J.F. Scott, K.S. Knight, S. Tarantino, A.M. Glazer, V. Shuvaeva, P. Daniel, M. Zhang, M.A. Carpenter, Phys. Rev. B **72**, 054110 (2005)
24. R. Sum, H.P. Lang, H.J. Güntherodt, Physica C **242**, 174 (1995)
25. S. Bueble, K. Knorr, E. Brecht, W.W. Schmahl, Surf. Sci. **400**, 345 (1998)
26. K. Daoudi, T. Tsuchiya, I. Yamaguchi, T. Manabe, S. Mizuta, J. Appl. Phys. **98**, 013507 (2005)
27. F. Laviano, L. Gozzellino, E. Mezzetti, P. Przyslupski, A. Tsarev, A. Wisniewski, Appl. Phys. Lett. **86**, 152501 (2005)
28. R. Desfeux, S. Bailleul, A. Da Costa, W. Prellier, A.M. Haghiri Gosnet, Appl. Phys. Lett. **78**, 3681 (2001)
29. A. Hammouche, E. Siebert, A. Hammou, Mater. Res. Bull. **24**, 367 (1989)
30. Wenbin Wu, K.H. Wong, C.L. Choy, J. Phys. D: Appl. Phys. **32**, L57 (1999)
31. E. Favre-Nicolin, Ph.D. thesis, Universitè Grenoble I - Joseph Fourier, 2003
32. A.Yu. Petrov, C. Aruta, S. Mercone, C. Adamo, I. Alessandri, L. Maritato, Eur. Phys. J. B **40**, 11 (2004)
33. K. Aizu, Phys. Rev. B **2**, 754 (1970)
34. J.H. Song, K.K. Kim, Y.J. Oh, H.J. Jung, J.H. Song, D.K. Choi, W.K. Choi, Journal of Crystal Growth **223**, 129 (2001)
35. A. Chiodoni, L. Gozzelino, F. Laviano, P. Przyslupski, A. Tsarev, A. Wisniewski, Phys. St. Sol. C **2**, 1644 (2005)
36. K. Vlasko-Vlasov, Y.K. Lin, D. J. Miller, U. Welp, G.W. Crabtree, V.I. Nikitenko, Phys. Rev. Lett. **84**, 2239 (2000)
37. J.A. Mydosh, *Spin glasses - An experimental introduction* (Taylor and Francis, London, UK, 2003)
38. A.H. Morrish, *The Physical Principles of Magnetism* (IEEE Press, New York, 2001)
39. H. Zijlstra, *Experimental Methods in Magnetism* (North-Holland, Amsterdam, 1967), Vol. 2
40. C.A. Perroni, V. Cataudella, G. De Filippis, G. Iadonisi, V. Marigliano Ramaglia, F. Ventriglia, Phys. Rev. B **68**, 224424 (2003)
41. Q. Yuan, e-print `arXiv:cond-mat/0112480`, unpublished
42. M. Medarde, J. Mesotr, P. Lacorre, S. Rosenkranz, P. Fisher, K. Gobrecht, Phys. Rev. B **52**, 9248 (1995)
43. M.E. Fisher, M.N. Barber, Phys. Rev. Lett. **28**, 1516 (1972)
44. M.N. Barber, in *Phase Transition and Critical Phenomena*, edited by C. Domb, J. Lebowitz (Academic Press, NY, 1983)
45. D. Fuchs, T. Schwarz, O. Moran, P. Schweiss, R. Schneider, Phys. Rev. B **71**, 092406 (2005)
46. C.S. Xiong, Y.H. Xiong, W. Yi, G.N. Meng, Z.C. Xia, X.G. Li, S.L. Yuan, J. Phys.: Condens. Matter **14**, 4309 (2002)
47. A. Ito, Riken Review No. 27, 18 (2000)
48. T. Zhu, B.G. Shen, J.R. Sun, H.W. Zhao, W.S. Zhan, Appl. Phys. Lett. **78**, 3863 (2001)
49. X.S. Wu, W. Cai, X.P. Zhang, Y.G. Zhao, L. Lu, J. Phys.: Condens. Matter **17**, 6981 (2005)
50. E. Dagotto, T. Hotta, A. Moreo, Phys. Rep. **344**, 1 (2001)
51. J. Deisenhofer, D. Braak, H.-A. Krug von Nidda, J. Hemberger, R.M. Eremina, V.A. Ivanshin, A.M. Balbashov, G. Jug, A. Loidl, 1 T. Kimura, Y. Tokura, Phys. Rev. Lett. **95**, 257202 (2005)
52. N. Mannella, A. Rosenhahn, C.H. Booth, S. Marchesini, B.S. Mun, S.H. Yang, K. Ibrahim, Y. Tomioka, C.S. Fadley, Phys. Rev. Lett. **92**, 166401 (2004)
53. F. Tsui, M.C. Smoak, T.K. Nath, C.B. Eom, Appl. Phys. Lett. **76**, 2421 (2000)
54. D.P. Pappas, K.P. Kämper, H. Hopster, Phys. Rev. Lett. **64**, 3179 (1990)
55. A.S. Moskvin, E.V. Zenkov, Yu.P. Sukhorukov, E.V. Mostovshchikova, N.N. Loshkareva, A.R. Kaul, O.Yu. Gorbenko, J. Phys.: Condens. Matter **15**, 2635 (2003)
56. J.S. Park, H.K. Lee, H.R. Bae, Y.P. Lee, J. Appl. Phys. **95**, 7100 (2004)
57. M. Fäth, S. Freisem, A.A. Menovsky, Y. Tomioka, J. Aarts, J.A. Mydosh, Science **285**, 1540 (1999)